

# 3-D MIMO-SAR Imaging Using Multi-Chip Cascaded Millimeter-Wave Sensors

Muhammet Emin Yanik<sup>1</sup>, Dan Wang<sup>2</sup>, and Murat Torlak<sup>1</sup>

<sup>1</sup>Dept. of Electrical and Computer Engineering, The University of Texas at Dallas, Richardson, TX, United States

<sup>2</sup>Radar and Analytics, Texas Instruments, Dallas, TX, United States

**Abstract**—Integration of multi-chip cascaded multiple-input multiple-output (MIMO) millimeter-wave (mmWave) sensors with synthetic aperture radar (SAR) imaging will enable cost-effective and scalable solutions for a variety of applications including security, automotive, and surveillance. In this paper, the first three-dimensional (3-D) holographic MIMO-SAR imaging system using cascaded mmWave sensors is designed and implemented. The challenges imposed by the use of cascaded mmWave sensors in high-resolution MIMO-SAR imaging systems are discussed. Especially, important signal processing functions such as near-field multistatic image reconstruction suitable for large MIMO apertures, multi-channel array calibration, spatial sampling, and image resolution are presented in the context of 3-D MIMO-SAR imaging. The prototyped 3-D MIMO-SAR imaging system is described in detail, along with various real imaging results.

**Index Terms**—millimeter-wave (mmWave), multiple-input multiple-output (MIMO), synthetic aperture radar (SAR), three-dimensional (3-D) imaging.

## I. INTRODUCTION

During the last decade, the progress in system-on-chip complementary metal-oxide semiconductor (CMOS) based frequency-modulated continuous-wave (FMCW) millimeter-wave (mmWave) sensors has resulted in the realization of cost-effective mmWave imaging solutions [1], [2]. A single-chip multiple-input-multiple-output (MIMO) mmWave sensor typically consists of a handful of transmitter and receivers. As a result, multiple sensor chips must be cascaded to create moderately large array apertures [3]. Even then, the number of chips that can be cascaded is limited due to the integration complexity of all the radio-frequency (RF) functionality required by a large number of transceiver channels into compact form factors. For applications such as creating an efficient three-dimensional (3-D) holographic image reconstruction of a target scene can still be challenging for cascaded MIMO sensors.

In this paper, we consider a hybrid concept based on the combination of synthetic aperture radar (SAR) technique and cascaded MIMO sensors to lower hardware complexity compared to fully electronic sampling solutions [4], [5]. In [1], we presented a two-dimensional (2-D) MIMO-SAR imaging system based on a single-chip mmWave sensor. In this paper, our goal is to exploit the wideband capabilities of mmWave sensors as well as cascaded sensor configuration to perform 3-D MIMO-SAR imaging.

On the other hand, the standard approaches such as Fourier-based image reconstruction framework using monostatic sampling schemes [6], [7] cannot be directly used for the MIMO-SAR configurations. The main reason is that one has to take into account the different trajectories of the incident and reflected electric fields for transceiver pairs due to increased separation among them. As a result, the image reconstruction techniques based on multistatic imaging modalities are necessary for the cascaded MIMO sensors with larger array apertures.

In this paper, we present a near-field reconstruction technique suitable for MIMO-SAR configurations. The presented technique first efficiently converts the measurement data from multistatic to monostatic, and then performs a holographic image reconstruction by augmenting the existing Fourier-based methods [8], [9].

More importantly, we build a MIMO-SAR imaging prototype based on the cascaded mmWave sensors and provide real imaging results to demonstrate the effectiveness of the complete solution in high-resolution 3-D holographic imaging applications. The cascaded MIMO radar is mounted on a two-axis fully controllable rail platform that synthesizes an aperture in both horizontal and vertical directions.

The rest of the paper is organized as follows: The complete 3-D MIMO-SAR image reconstruction framework, including the signal model, system configuration, and the proposed algorithm is discussed in Section II. Section III presents the hardware architecture of the prototyped imager. Real imaging results are reported in Section IV, which is followed by conclusions.

## II. 3-D MIMO-SAR IMAGE RECONSTRUCTION

### A. Beat Signal in the Wavenumber Domain

We develop our signal model based on the mmWave radar sensors that use FMCW signals. Assuming an FMCW signal is backscattered from a single point on the target, it returns to the receiver element in the delayed and scaled version of the transmitted signal. The radar then demodulates the received signal by mixing it with a copy of the transmitted signal, which is known as dechirping that results in a complex beat (or intermediate frequency) signal [10]

$$s(t) = \sigma e^{j2\pi(f_0\tau + K\tau t - 0.5K\tau^2)}, \quad 0 \leq t \leq T, \quad (1)$$

where  $\sigma$  is the combination of target reflectivity of  $p$  and the round-trip amplitude decay [11],  $f_0$  is the carrier frequency at time  $t = 0$ ,  $K = B/T$  is the slope of frequency computed from the sweep bandwidth of  $B$ , and the signal duration of  $T$ . Assuming the distance associated with the transmitter element and the receiver element to a point scatterer as  $R_T$  and  $R_R$ , respectively, the round-trip delay of the echo in (1) can be calculated as  $\tau = (R_T + R_R)/c$ , where  $c$  is the speed of light. The last term of (1) is known as the residual video phase (RVP), which is found to be negligible [12]. Ignoring the round-trip amplitude decay, the beat signal can be rewritten in the wavenumber domain as

$$s(k) = p e^{jk(R_T+R_R)}, \quad (2)$$

where  $k = 2\pi f/c$  is the wavenumber corresponding to the frequency  $f = f_0 + Kt$ .

### B. MIMO-SAR Configuration

In this paper, a 2-D SAR aperture is synthesized by mechanically moving a cascaded MIMO sensor in a parallel track pattern, as shown in Fig. 1. In the established  $(x, y, z)$  Cartesian coordinate system,  $x$ -axis,  $y$ -axis, and  $z$ -axis denote horizontal, vertical, and depth directions, respectively. In [1], we presented a 2-D SAR imaging system with similar configuration based on a single-chip MIMO sensor with limited dimensions and scanning speed.

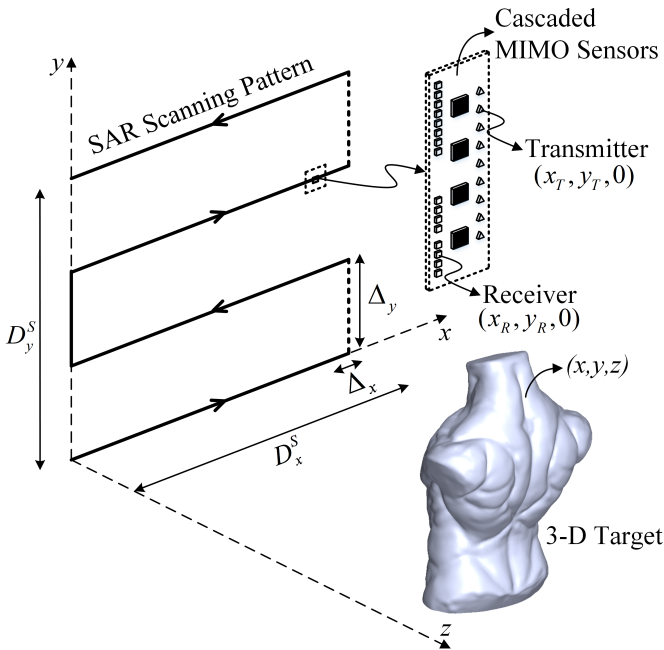


Fig. 1: A 3-D target is illuminated using a cascaded MIMO sensor on the mechanical scanner follows a rectangular trajectory.

If a 3-D target is characterized by its reflectivity function  $p(x, y, z)$ , the main purpose of the MIMO-SAR imaging scheme is to recover  $p(x, y, z)$  from the five-dimensional

(5-D) received data  $s(x_T, y_T, x_R, y_R, k)$  captured by each transceiver pair over the  $xy$ -domain.

### C. Multistatic-to-Monostatic Conversion

Under far-field assumptions, a multistatic array topology with  $M_T + M_R$  physical antennas can be transformed to a monostatic virtual array with  $M = M_T \times M_R$  elements by the effective phase center principle. However, in near-field operations, to adopt the existing Fourier-based image reconstruction techniques based on monostatic sampling schemes [6], [7] for multistatic imaging systems with large MIMO apertures, a more accurate conversion operation is needed.

Let us denote the location of the phase center associated with the transmitter element at  $(x_T, y_T, 0)$  and the receiver element at  $(x_R, y_R, 0)$  as  $(x', y', 0)$ . Defining a reference point  $(x_0, y_0, z_0)$  at the center of the target domain, the received multistatic data set  $s(x_T, y_T, x_R, y_R, k)$  can be converted to the effective monostatic version as [8], [9]

$$\hat{s}(x', y', k) = s(x_T, y_T, x_R, y_R, k) \frac{\hat{s}_0(x', y', k)}{\hat{s}_0(x_T, y_T, x_R, y_R, k)}, \quad (3)$$

where

$$\begin{aligned} \hat{s}_0(x_T, y_T, x_R, y_R, k) &= e^{jk(\hat{R}_T + \hat{R}_R)} \\ \hat{s}_0(x', y', k) &= e^{j2k\hat{R}}, \end{aligned} \quad (4)$$

are the recorded data from the multistatic and the corresponding monostatic array, respectively. We assume that a target domain contains only a point scatterer at the reference point. In (4),  $\hat{R}_T$  and  $\hat{R}_R$  are the distances from transmit and receive antennas to the reference point, respectively; and  $\hat{R}$  is the distance between the corresponding phase center and the reference point. Using the approximation developed in [1], (3) can be further simplified as

$$\hat{s}(x', y', k) = s(x_T, y_T, x_R, y_R, k) e^{-jk\left(\frac{d_x^2 + d_y^2}{4z_0}\right)}, \quad (5)$$

where  $d_x$  and  $d_y$  are the distances between the transmitter and receiver elements along  $x$  and  $y$  axes, respectively.

### D. 3-D Image Reconstruction Algorithm

Here, we review the existing monostatic SAR image reconstruction techniques [6], [7], which form the basis of our MIMO-SAR image formation process after implementing the multistatic-to-monostatic conversion detailed in Section II-C. Dropping the distinction between the primed and unprimed coordinate system as they coincide, the image reconstruction can be carried out as

$$p(x, y, z) = \text{IFT}_{3D}^{(k_x, k_y, k_z)} \left[ \text{Stolt}^{(k)} \left( \text{FT}_{2D}^{(x, y)} [\hat{s}^*(x, y, k)] \right) \right], \quad (6)$$

where  $(.)^*$  denotes the complex-conjugate operation,  $\text{FT}_{2D}^{(x, y)}(.)$  denotes 2-D Fourier transform operation over

the  $xy$ -domain,  $\text{Stolt}^{(k)}(\cdot)$  denotes the Stolt interpolation [7], [13] to resample the  $k$ -domain data to uniformly spaced positions in  $k_z$ -domain using (7), which divides the wavenumber  $k$  into three components  $k_x$ ,  $k_y$ , and  $k_z$  in the Cartesian coordinate system according to the dispersion relation for plane waves

$$k_z = \sqrt{4k^2 - k_x^2 + k_y^2}, \quad k_x^2 + k_y^2 \leq (2k)^2, \quad (7)$$

and  $\text{IFT}_{3D}^{(k_x, k_y, k_z)}(\cdot)$  denotes 3-D inverse Fourier transform operation over the  $k_x k_y k_z$ -domain.

In the proposed MIMO-SAR imaging system, the reflected signal from the target is discretely sampled on the continuous aperture plane using an  $M$  element uniform virtual MIMO array, where the virtual elements are uniformly spaced along the  $y$ -axis by  $\lambda/4$ , which satisfies the Nyquist criterion for the worst-case scenario [6]. As depicted in Fig. 1, the 2-D SAR aperture is uniformly sampled in  $x$  spatial domain with a sampling distance of  $\Delta_x$ . Using the virtual channel concept, and selecting the sampling distance in  $y$ -axis as  $\Delta_y = M\lambda/4$ , the 2-D SAR aperture becomes uniformly sampled in  $y$  spatial domain also. The total effective aperture sizes in both axes is then approximated by  $D_x \approx (N_x - 1)\lambda/4$  and  $D_y \approx N_y(M - 1)\lambda/4$ , where  $N_x$  is the total number of measurement points along  $x$ -axis, and  $N_y$  is the total number of vertical scans along  $y$ -axis. Using the approximated effective aperture size, the cross-range image resolutions can be estimated as given in [4], [11].

### III. EXPERIMENTAL SETUP

The prototyped system shown in Fig. 2 consists of a cascaded mmWave sensor from Texas Instruments [14], a two-axis mechanical scanner, a motor controller, and a host personal computer (PC). The diagram shown in Fig. 3 is a simplified view of the main elements and the high-level system architecture of the imaging system. Both radar and rail system are controlled via a MATLAB graphical user interface (GUI).

The cascaded MIMO radar is a combination of four AWR1243 mmWave sensors and add-on interface boards to enable high-speed raw data capture for post-processing. A single AWR1243 mmWave radar chip has four receive and three transmit antennas with a 4 GHz frequency bandwidth from 77 GHz to 81 GHz. Our goal here is to exploit the available 4 GHz bandwidth to facilitate 3-D image reconstruction.

A sketch of the physical antenna layout is shown in Fig. 3. The transmit antennas from three chips are uniformly spaced along  $y$ -axis by  $2\lambda$  (tuned to the frequency of 77 GHz). The remaining three transmit antennas (not shown in Fig. 3) from one of the chips have offsets along  $x$ -axis. The receive antennas connected to each chip are grouped and uniformly spaced in  $y$ -axis by  $\lambda/2$ . With this configuration, a virtual array of 86 channels along the vertical direction is achieved [14]. The orthogonality between the transmit antennas is achieved by employing time division multiplexing (TDM) technique.



Fig. 2

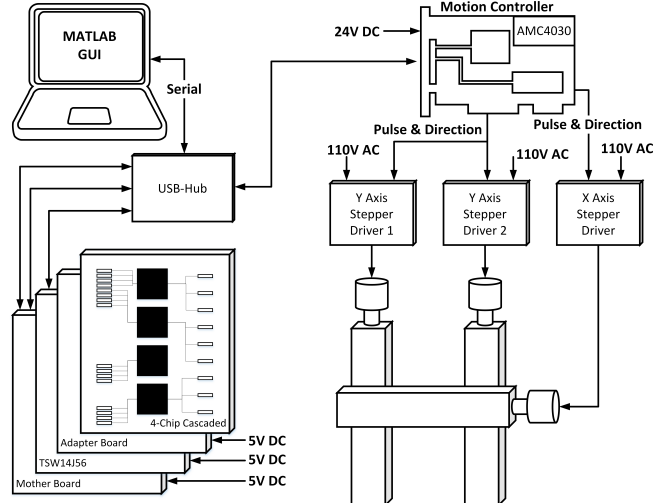


Fig. 3: Architecture of mmWave imager prototype.

The other component of the prototyped system is the two-axis mechanical scanner built using linear rails and stepper motors. The scanner provides movements in horizontal and vertical directions. The maximum scanning ranges in both axes are 1000 mm. The motor controller, which is configured to operate linear rails at a maximum speed of 400 mm/s, is connected to the host PC with a serial port.

### IV. IMAGING RESULTS

To verify the effectiveness of the cascaded mmWave sensor based imaging prototype, the experimental image results of uncovered and concealed targets are provided. In all experiments, FMCW waveforms are configured to vary from  $f_0 =$

77.38 GHz to  $f_T = 80.93$  GHz, where the signal duration  $T \approx 56 \mu\text{s}$  and the frequency slope  $K \approx 70.3 \text{ MHz}/\mu\text{s}$ . The spatial sampling intervals are selected as  $\Delta_x = \lambda/4 \approx 1 \text{ mm}$  and  $\Delta_y = 86\lambda/4 \approx 83 \text{ mm}$  along  $x$  and  $y$  axes, respectively.

In the first experiment, a small test target with a size of 100 mm by 150 mm is cut out from a copper-clad laminate as shown in Fig. 4a. In this scenario, the target is placed at a distance of  $z_0 \approx 395 \text{ mm}$  from the scanner. The SAR aperture is synthesized to cover an area of  $D_x^S \approx 500 \text{ mm}$  ( $N_x = 500$ ) by  $D_y^S \approx 500 \text{ mm}$  ( $N_y = 6$ ). This configuration provides the lateral resolution of about 1.5 mm.

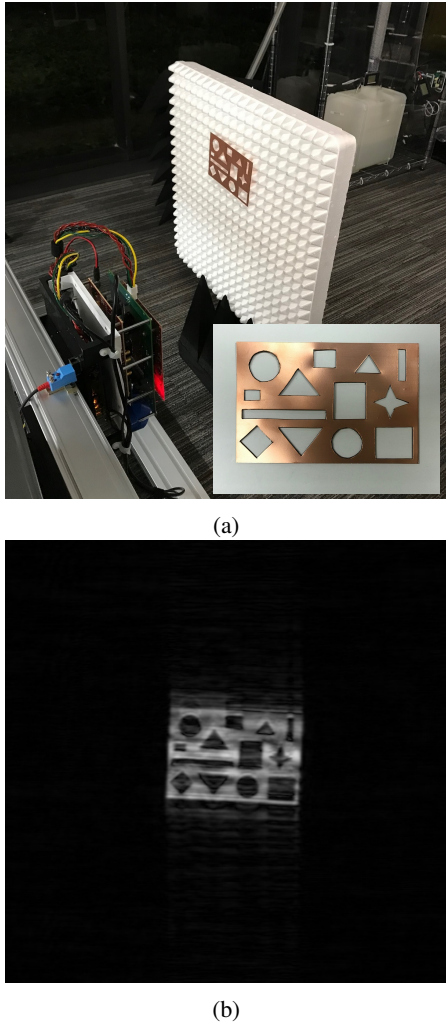


Fig. 4: Imaging scenario with the test target: (a) optical image, and (b) reconstructed 3-D image (front view).

The imaging scenario in Fig. 5a shows a pair of scissors concealed in a cardboard box. In this scenario, the target is placed at a mean distance of  $z_0 \approx 250 \text{ mm}$  from the scanner. The SAR aperture is synthesized to cover an area of  $D_x^S \approx 500 \text{ mm}$  ( $N_x = 500$ ) by  $D_y^S \approx 500 \text{ mm}$  ( $N_y = 6$ ). The lateral resolution achieved in this configuration is about 1 mm.

The minor artifacts in the experiments are caused by some residual calibration errors. In this paper, we adopted the array

calibration technique presented in [1] for the cascaded MIMO radar. The calibration process is very critical for the quality of images. The complexity increases with the array size. We are working on more effective and efficient calibration approaches to improve the imaging quality for large MIMO apertures. We will report our results in a future article.

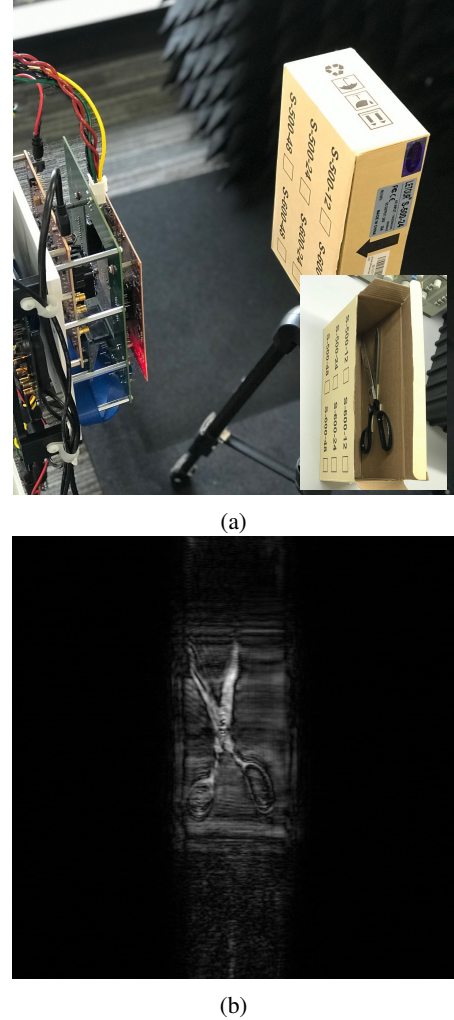


Fig. 5: Imaging scenario with the scissors concealed in a cardboard box: (a) optical image, and (b) reconstructed 3-D image (front view).

## V. CONCLUSION

In this paper, we presented a 3-D MIMO-SAR imaging system utilizing multi-chip cascaded mmWave sensors. We developed a complete system, including a computationally efficient image reconstruction algorithm based on a multistatic-to-monostatic conversion. Imaging results obtained using the prototyped system demonstrate the effectiveness of this system for the identification of objects enclosed in boxes.

## ACKNOWLEDGMENT

This work is supported by Semiconductor Research Corporation (SRC) task 2712.029 through The University of

Texas at Dallas' Texas Analog Center of Excellence (TxACE). The authors would like to thank Adeel Ahmad from Texas Instruments for his valuable comments and support for this work.

## REFERENCES

- [1] M. E. Yanik and M. Torlak, "Near-field MIMO-SAR millimeter-wave imaging with sparsely sampled aperture data," *IEEE Access*, vol. 7, pp. 31 801–31 819, Mar. 2019.
- [2] ——, "Near-field 2-D SAR imaging by millimeter-wave radar for concealed item detection," in *Proc. IEEE Radio and Wireless Symp.*, Orlando, FL, USA, Jan. 2019, pp. 1–4.
- [3] Building cascade radar using TI's mmwave sensors, Texas Instruments. [Online]. Available: <https://training.ti.com/build-cascaded-radar-using-tis-mmwave-sensors>
- [4] X. Zhuge and A. G. Yarovoy, "A sparse aperture MIMO-SAR-based UWB imaging system for concealed weapon detection," *IEEE Trans. on Geoscience and Remote Sensing*, vol. 49, no. 1, pp. 509–518, Jan. 2011.
- [5] R. Zhu, J. Zhou, G. Jiang, and Q. Fu, "Range migration algorithm for near-field MIMO-SAR imaging," *IEEE Geoscience and Remote Sensing Letters*, vol. 14, no. 12, pp. 2280–2284, Dec. 2017.
- [6] D. M. Sheen, D. L. McMakin, and T. E. Hall, "Three-dimensional millimeter-wave imaging for concealed weapon detection," *IEEE Trans. on Microwave Theory and Techniques*, vol. 49, no. 9, pp. 1581–1592, Sep. 2001.
- [7] J. M. Lopez-Sanchez and J. Fortuny-Guasch, "3-D radar imaging using range migration techniques," *IEEE Trans. on Antennas and Propagation*, vol. 48, no. 5, pp. 728–737, May 2000.
- [8] W. F. Moulder, J. D. Krieger, J. J. Majewski, C. M. Coldwell, H. T. Nguyen, D. T. Maurais-Galejs, T. L. Anderson, P. Dufilie, and J. S. Herd, "Development of a high-throughput microwave imaging system for concealed weapons detection," in *Proc. IEEE Int. Symp. on Phased Array Systems and Technology*, Waltham, MA, USA, Oct. 2016, pp. 1–6.
- [9] Z. Wang, Q. Guo, X. Tian, T. Chang, and H. Cui, "Near-field 3-D millimeter-wave imaging using MIMO RMA with range compensation," *IEEE Trans. on Microwave Theory and Techniques*, vol. 67, no. 3, pp. 1157–1166, Mar. 2019.
- [10] A. Meta, P. Hoogeboom, and L. P. Ligthart, "Signal processing for FMCW SAR," *IEEE Trans. on Geoscience and Remote Sensing*, vol. 45, no. 11, pp. 3519–3532, Nov. 2007.
- [11] X. Zhuge and A. G. Yarovoy, "Three-dimensional near-field MIMO array imaging using range migration techniques," *IEEE Trans. on Image Processing*, vol. 21, no. 6, pp. 3026–3033, Jun. 2012.
- [12] G. Wang, J. Muñoz-Ferreras, C. Gu, C. Li, and R. Gómez-García, "Application of linear-frequency-modulated continuous-wave (LFMCW) radars for tracking of vital signs," *IEEE Trans. on Microwave Theory and Techniques*, vol. 62, no. 6, pp. 1387–1399, Jun. 2014.
- [13] R. H. Stolt, "Migration by Fourier transform," *Geophysics*, vol. 43, no. 1, pp. 23–48, Feb. 1978.
- [14] Imaging radar using cascaded mmwave sensor reference design. [Online]. Available: <http://www.ti.com/tool/TIDEP-01012>